Classification of Mild Cognitive Impairment With Multimodal Data Using Both Labeled and Unlabeled Samples

Shaoxun Yuan, Haitao Li, Jiansheng Wu, and Xiao Sun

Abstract—Mild Cognitive Impairment (MCI) is a preclinical stage of Alzheimer's Disease (AD) and is clinical heterogeneity. The classification of MCI is crucial for the early diagnosis and treatment of AD. In this study, we investigated the potential of using both labeled and unlabeled samples from the Alzheimer's Disease Neuroimaging Initiative (ADNI) cohort to classify MCI through the multimodal co-training method. We utilized both structural magnetic resonance imaging (sMRI) data and genotype data of 364 MCI samples including 228 labeled and 136 unlabeled MCI samples from the ADNI-1 cohort. First, the selected quantitative trait (QT) features from sMRI data and SNP features from genotype data were used to build two initial classifiers on 228 labeled MCI samples. Then, the co-training method was implemented to obtain new labeled samples from 136 unlabeled MCI samples. Finally, the random forest algorithm was used to obtain a combined classifier to classify MCI patients in the independent ADNI-2 dataset. The experimental results showed that our proposed framework obtains an accuracy of 85.50 percent and an AUC of 0.825 for MCI classification, respectively, which showed that the combined utilization of sMRI and SNP data through the co-training method could significantly improve the performances of MCI classification.

Index Terms—Mild cognitive impairment, classification, co-training, sMRI, SNP

1 Introduction

Alzheimer's Disease (AD) is a progressive and irreversible complex neurodegenerative disease with responsible for about half a million deaths worldwide per year [1]. Mild Cognitive Impairment (MCI) is considered as a preclinical stage of AD. MCI has clinical heterogeneity [2]. Some MCI patients will stay stable (stable MCI, sMCI) after 10-years' follow-up or even return to normal cognitive status by timely interventions [3], [4]. Other patients will progress to AD (progressive MCI, pMCI) after a period of time [5] and will die after more than three years [6]. Therefore, the classification of MCI is necessary and urgent for identification and effective therapeutic interventions of early AD.

For AD and normal control (NC) classification, good performances have been reported in many studies. Sun *et al.* [7] presented an accuracy of 92.8 percent on AD/NC classification using gray matter density, Zhu *et al.* [8] acquired a 90.3 percent accuracy using gray matter volume. Compared to AD/NC classifications, the performances of sMCI/pMCI classification are much lower. Davatzikos *et al.* [9] reported an accuracy of 56 percent in the classification of MCI samples using structural magnetic resonance imaging (sMRI) data from the Alzheimer's Disease Neuroimaging Initiative (ADNI) cohort, while the sensitivity was quite high (95 percent) and specificity was quite low (38 percent). Sun *et al.* [7] reported an accuracy of 64 percent using gray matter density map, Salvatore *et al.* [10] reported an accuracy of 62 percent using single sMRI feature, Zhu *et al.* [11] obtained an accuracy 71.3 percent using gray matter volumes.

Structural imaging findings are classification markers for neurodegenerative disease. Quantitative trait (QT) markers based on sMRI are sensitive to reflect the first morphological changes in the AD brain [12] and have been proved to be associated with MCI progression [13]. Compared with the computed tomography (CT) and positron emission tomography (PET), sMRI has the advantages of high-quality spatial resolution, sufficient contrast, completely non-invasive and lower cost. Medial temporal lobe atrophy extracted from sMRI can be used as an imaging biomarker of AD, and the accuracy of distinguishing AD patients from normal people is up to 89 percent [14]. MCI is image heterogeneity. Fleisher *et al.* [15] found that the brain atrophy pattern of MCI patients is consistent with that of AD patients, that is, the structural changes in the medial temporal lobe make MCI patients more likely to progress to AD, while Karas *et al.* [16] found that MCI patients with atrophy of the left temporal lobe parietal lobe and other structures are more likely to progress to AD. Chupin *et al.* [17] found that hippocampal volume was a potential imaging marker for predicting whether a MCI patient will convert to AD after 18 months. Querbes *et al.* [18] found that cortical thickness could predict MCI progression after 24 months.

- *Shaoxun Yuan, Haitao Li, and Xiao Sun are with the State Key Laboratory of Bioelectronics, School of Biological Science and Medical Engineering, Southeast University, Nanjing 210096, P.R. China. E-mail: {230159460, leehightall, xsun}@seu.edu.cn.*
- *Jiansheng Wu is with the Department of Geographic and Biologic Information, Nanjing University of Posts and Telecommunications, Nanjing 210003, China. E-mail: jansen@njupt.edu.cn.*

Manuscript received 14 Mar. 2020; revised 30 Dec. 2020; accepted 16 Jan. 2021. Date of publication 20 Jan. 2021; date of current version 8 Dec. 2021.
(Corresponding author: Xiao Sun.)
Digital Object Identifier no. 10.1109/TCBB.2021.3053061

Genetic factors play important roles in the pathogenesis of MCI and AD. Genetic factors contribute up to 79 percent to the incidence of AD [19] and *APOE* ε4 is the most significant risk factor of AD. MCI is a genetically complex disease and there is no major risk genetic factor known to be related to MCI [20]. Some studies have shown that *APOE* ε4 is correlated with the high risk of MCI [21], while the correlation was not confirmed in other studies [22], [23]. Meanwhile, the roles of some well-known AD-related loci in MCI are not clear. Single nucleotide polymorphism (SNP) can be used as features for classification. Ning *et al.* reported the ability of AD risk loci in AD/NC classification [24]. Rodríguez *et al.* [25] selected 8 known AD-related loci and found there was no good discrimination for the classification of MCI.

Multimodal data could reflect the biological mechanism of AD and MCI from different views, and also could provide complementary information in classifications which is robust to noise and data heterogeneity [26]. Several studies combined multimodal data to improve classification performance. Liu *et al.* [27] combined MRI and PET data through convolutional neural networks in AD/NC classification and the accuracy of multimodality (93.26 percent) was higher than single modality (84.97 percent of MRI and 88.08 percent of PET). Supervised learning and unsupervised learning are the two major directions of traditional machine learning [28]. Supervised learning requires all samples are labeled, while unsupervised learning does not. However, the collection of labeled samples is expensive and time-consuming in practice. Semi-supervised learning (SSL) combines labeled and unlabeled samples to improve the generalization ability and performances of classifiers. Unlabeled samples could be used to estimate the intrinsic geometric structure of the actual data [29] and also can provide feature information during the construction of the classification models. Wu *et al.* [30] used SSL in diabetes disease diagnostic study, and prediction accuracy was 82.29 percent compared to the supervised learning classifier with an accuracy of 79.17 percent. An *et al.* [31] regarded MCI as unlabeled samples in AD/NC prediction and obtained a 1-2 percent improvement in accuracy compared with the state-of-the-art method. Co-training is a representative algorithm of SSL, which trains two separately classifiers on two sufficient and redundant views [32], that is, each view is sufficient to learn a classifier and these two views are mutually independent. Sun *et al.* [33] used labeled and unlabeled data in breast cancer diagnosis through co-training, and the AUC was 7.4 percent higher than using labeled data only.

To our knowledge, no study has actually considered both labeled and unlabeled samples to classify MCI from multimodal views. In this study, we investigated the possibility of using both labeled and unlabeled MCI samples in the ADNI cohort through co-training to help to classify MCI samples with multimodal data including baseline sMRI and SNP data. First, we built two separated initial classifiers using selected QT and SNP features on original labeled MCI samples derived from the ADNI-1 cohort. Then, unlabeled MCI samples from the ADNI-1 cohort were used in the co-training processes. Finally, random forest (RF) was used to obtain a combined classifier. MCI samples from the ADNI-2 dataset were applied to evaluate the effectiveness of the methods. The workflow of our research is illustrated in Fig. 1.

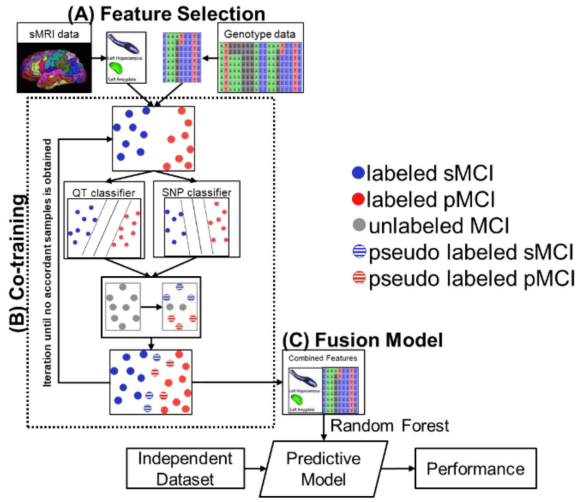

Fig. 1. The workflow of our proposed methods. (A) Feature selection. QT and SNP features are selected from sMRI and genotype data, respectively. SVM is utilized to build initial QT and SNP classifiers using the selected features. (B) Co-training. Unlabeled MCI samples are used in the co-training processes. Two classifiers classify the unlabeled MCI samples and the accordant pseudo labeled sMCI and pMCI samples are added to the labeled MCI samples. (C) Fusion Model. The random forest algorithm is used to obtain a combined classifier. ADNI-2 cohort is used as an independent dataset to evaluate the performance of our predictive model.

2 Materials and Methods

2.1 Data Description

Data used in the preparation of this article were obtained from the ADNI database (adni.loni.usc.edu). As such, the investigators within the ADNI contributed to the design and implementation of ADNI and/or provided data but did not participate in analysis or writing of this report. The ADNI was launched in 2003 as a public-private partnership, led by Principal Investigator Michael W. Weiner, MD. The primary goal of ADNI has been to test whether serial MRI, PET, other biological markers, and clinical and neuropsychological assessment can be combined to measure the progression of MCI and early AD.

2.2 Samples

We used ADNI sample data collected from 50 clinic sites. A total of 819 individuals were recruited by the ADNI-1 cohort, and 757 of them were run on the Human610-Quad BeadChip for genotype data and underwent high-resolution T1-weighted Magnetization Prepared Rapid Gradient Echo (MP-RAGE) structural MRI at baseline. Among these 757 individuals, 364 individuals were categorized as MCI samples at baseline according to the records from ADNI database. In the ADNI-2 cohort, 290 individuals were run on the Illumina HumanOmniExpress BeadChip for genotype data and underwent high resolution T1-weighted MP-RAGE structural MRI at baseline, of which 146 individuals were categorized as MCI samples at baseline according to the records from ADNI database. In this study, those MCI samples progressed to AD after 36-months' were identified as pMCI and those MCI samples remained MCI during the 36 months' observation time were identified as sMCI. sMCI and pMCI samples were considered as labeled MCI samples. Meanwhile, other MCI samples were identified as

unlabeled MCI (uMCI) due to lack of 36-month' follow-up diagnostic information or diagnoses fluctuate. Diagnose fluctuate can be defined as a sample may wobbly among cognitive status [34] or diagnosis fluctuation between different trajectories of MCI (e.g., progressing from MCI to dementia, but back to MCI) within a certain follow-up time period [35].

The following data of all samples were obtained: T1-weighted MRI, the Illumina SNP genotyping data, and clinical information of patients including gender, age, years of education, the Mini-Mental State Examination (MMSE) score, and the Clinical Dementia Rating Sum of Boxes (CDR-SB) score. The MMSE [36] is a quick and easy measurement for cognitive dysfunction with scores that range from 0 to 30, and the CDR-SB [37] is a clinician-rated staging method that ranges from 0 to 3. Subjects with lower MMSE scores or higher CDR-SB scores indicate greater cognitive dysfunctions. Student's t-test was used to assess the statistical significant differences of age, education year, MMSE score, and CDRSB score between the sMCI and the pMCI groups in ANDI-1 cohort.

2.3 Image and Genotype Data Pre-Processing

A total of 103 QT, including 35 subcortical structure volumes and 68 cortical structure thicknesses were measured from T1-MRI images using Freesurfer (Version 6.0.0) [38] for all selected samples.

QT adjustments were performed due to individual brain differences [39]. A linear regression model [40] was used for raw QT adjustments by global measurement (GM), intracranial volume for subcortical structures, and cortical mean thickness for cortical structures, as described below (1). The adjusted QT of the ith structure (*ROIi adjusted)* of a sample was defined as,

$$ROI^{i}_{adjusted} = ROI^{i}_{raw} - \varepsilon_i(GM_{raw} - GM_{mean}), \quad (1)$$

ROIi adjusted represents the raw quantitative trait of the ith structure of the sample, GM_{raw} represents the global measurement of the sample and GM_{mean} represents the mean GM across all samples. $\boldsymbol{\varepsilon}_i$ is the slope of the regression line between *ROIi raw* and GM_{raw} across all MCI samples. Subcortical volume and cortical thickness were widely ranged and with different dimensions, so the standardization of origin data is needed. The Z-score method was used for data standardization.

The original genotype data of the ADNI-1 cohort contained 620901 markers on the Illumina Human610-Quad BeadChip. First, all CNV markers (21890) and SNP markers in non-autosomal chromosomes (16475) were excluded. Then, quality control procedures were performed using *PLINK* software (Version 1.70) [41]. SNPs with a call rate of less than 90 percent, or deviations from the Hardy-Weinberg Equilibrium [42] (5 × 10-7), or Minor Allele Frequency (MAF) less than 10 percent were excluded from the genotype dataset. 456028 SNPs remained after quality control. Finally, a binary-traits GWAS was conducted using sMCI and pMCI samples as negative and positive samples, respectively. Genotype clumping was conducted using *PLINK* software. We used the following clumping settings in *PLINK*: –clump-p1 5×10^{-4} –clump-p2 5×10^{-4} –clump-r2 0.5 –clump-kb 500 for genotype clumping. After clumping, 125 SNP loci significantly associated with MCI progress were kept and transcoded to 374 SNP features with the one-hot encoding [43] process (Fig. 2). The Manhattan plot of MCI progress-associated SNPs and the list of 125 significant SNP loci are supplemented in Figure S1 (Appendix A) and Table S1 (Appendix B), respectively, which can be found on the Computer Society Digital Library at http://doi.ieeecomputersociety.org/10.1109/TCBB.2021.3053061.

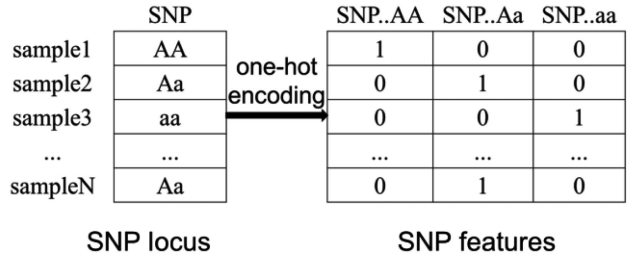

Fig. 2. SNP locus is transcoded to SNP features using one-hot encoding. Assuming A is the major allele and a is the minor allele of a SNP, there are three allele types of the SNP, AA, Aa, and aa. These categorical variables AA, Aa or aa were transcoding to discrete variables [10,0], [01,0] or [00,1].

2.4 Feature Selections and Classification of MCI

Feature selection is an important process that can remove irrelevant, redundant, and noisy features, and directly improve classification performances. Least Absolute Shrinkage and Selection Operator (Lasso) is a popular algorithm for feature selection which penalizes a linear regression model with *l1-norm* [44]. In this study, we used the R packaged names glmnet (version 2.0-18) to perform the Lasso method for feature selections. In each round of QT and SNP feature selections, we ran Lasso 100 times and features were ranked by frequency, and features with the same frequency were re-ranked use learning Vector Quantization (LVQ) approach [45]. The selected features of each modal data were based on the feature ranking results. (Fig. 1A). The initial QT and SNP classifiers were built on the ADNI-1 labeled MCI samples by SVM method using the selected QT and SNP features.

Co-training [32] is a semi-supervised machine learning method, with which multimodal features and unlabeled samples are used to improve the classification performances. Let L and U represent the labeled and unlabeled MCI datasets, respectively. f_{QT} and f_{SNP} represent the classifiers that were built on L using selected QT and SNP features, respectively. A subset (u) of unlabeled MCI samples were selected from U randomly and classified by f_{QT} and f_{SNP}, respectively. Unlabeled MCI samples classified by QT and SNP classifiers were considered as pseudo labeled MCI samples. s_{QT} and p_{QT} denote the pseudo labeled sMCI and pMCI samples which were classified by f_{QT} respectively, while s_{SNP} and p_{SNP} denote the pseudo labeled samples which were classified by f_{SNP} respectively ($s_{QT} \cup p_{QT} = s_{SNP} \cup p_{SNP} = u$). The accordant pseudo sMCI samples ($s_{QT} \cap s_{SNP}$) and pseudo pMCI samples ($p_{QT} \cap p_{SNP}$) were added to L and the discordant pseudo samples were released back to U. Such processes were iterated until the labels of selected pseudo samples were totally different predicted by the QT classifier and the SNP classifier. As

TABLE 1
The Demographic Characteristics of Selected Samples

	ADNI-1				ADNI-2	
	sMCI	pMCI	uMCI	p-Value	sMCI	pMCI
Number	115	113	136	-	62	21
Gender (F/M)	38/77	40/73	47/89	-	25/37	10/11
Age	74.47±7.27	74.89±6.67	74.85±7.87	0.65	69.61±6.28	72.61±5.35
Edu Year	15.81±2.98	15.85±2.97	15.42±3.13	0.92	16.22±2.54	16.48±2.67
MMSE	27.63±1.67	26.67±1.69	26.79±1.82	3.41×10^{-5}	28.19±1.53	27.67±1.67
CDRSB	1.33±0.63	1.79±0.99	1.69±0.90	2.70×10^{-5}	1.10±0.66	2.24±1.02

 # Age, education year, MMSE score, and CDRSB score are presented as mean ± standard deviation mode. P-values for differences between the sMCI group and the pMCI group are based on the t-test.

comparisons, we built five different models for the impacts of the different unlabeled sample chosen sizes u (10, 15, 20, 25, and 30) on model performances. The accordant sample sizes and the performances of the combined classifiers of each model are provided in Table S5 (Appendix D), available in the online supplemental material. Finally, we got new labeled MCI samples composed of L and accordant pseudo labeled MCI samples (Fig. 1B).

Subsequently, the random forest algorithm was used to obtain a combined classifier on the new labeled MCI samples (Fig. 1C). RF is a popular algorithm developed by Breiman that uses an ensemble of decision tree classifiers [46]. In our study, the selected QT and SNP features were combined, and the RF algorithm was used to obtain a combined classifier on the new labeled MCI dataset after the iterations were terminated. 83 MCI samples from the ADNI-2 were applied to evaluate the effectiveness of the combined classifier.

2.5 Methods of SNP Annotations

To identify the biological significance of the selected SNP loci and corresponding genes, we pursued the following strategies: (1) Ensemble VEP database was used to evaluate the potential effects of SNPs on genes, transcripts, protein sequences and regulatory regions in coding and non-coding regions [47]. (2) HaploReg database was used to explore the regulatory potential and the eQTL information of SNPs [48]. (3) The Braineac eQTL database was used to analyze the differences in transcriptomic expressions in ten brain regions (cerebellar cortex, frontal cortex, hippocampus, medulla, occipital cortex, putamen, substantia nigra, temporal cortex, thalamus, and white matter) among different genotypes of SNPs [49]. (4) Gene enrichment analysis was performed in STRING database [50].

3 Results and Discussion

3.1 Sample Statistics

MCI is heterogeneous. The criteria for distinguishing sMCI and pMCI are quite different. Westman *et al.* [51] categorized 256 sMCI and 62 pMCI according to the diagnostic information of 12-months' follow-up. Cho *et al.* [52] used 18-months' follow-up as the criterion and obtained 131 sMCI and 72 pMCI. Casanova *et al.* [53] used 36-months' follow-up and labeled 182 sMCI and 153 pMCI. Wolz *et al.* [54] categorized MCI samples into sMCI group if a sample was not progressed to AD as of July 2011, and other samples were considered as pMCI. In our views, diagnostic information should be considered at not only a defined time point but also those time points before the defined time point. Meanwhile, samples with diagnosis fluctuate also should not be considered as sMCI or pMCI arbitrary because clinical diagnosis information may be somewhat subjective. Thus in our study, 228 labeled MCI samples from the ADNI-1 cohort were categorized into 115 sMCI and 113 pMCI according to their diagnostic information at 36-months' follow-up, while other 136 MCI samples were considered as unlabeled MCI due to lack of follow-up diagnostic information or diagnosis fluctuate. 83 samples from the ADNI-2 cohort were grouped to 62 sMCI and 21 pMCI according to the previous criterion. The baseline demographic characteristics of all selected MCI samples were summarized in Table 1. In the ADNI-1 cohort, there was no significant difference in age and education year between the sMCI group and the pMCI group ($p = 0.65$, $p = 0.92$, respectively). The sMCI group had a significantly higher MMSE score and a significantly lower CDR-SB score than the pMCI group ($p = 3.41 \times 10^{-5}$, $p = 2.70 \times 10^{-5}$). The results indicated that the pMCI group showed marked cognitive dysfunctions compared to the sMCI group at baseline in the ADNI-1 cohort.

3.2 Selected Features for MCI Classification

Feature selection is a necessary mid-step, which can reduce computational complexity and improve model performance of machine learning. SNP features reveal molecular-level information, which is complementary to the brain tissue level information from sMRI data. In recent years, a large number of machine learning studies based on multimodal features have been applied in MCI and AD classification and obtained better classification performance than single modal method [55], [56], [57]. In our study, QT and SNP features were selected from 103 QT features derived from sMRI data and 374 SNP features derived from genotype data, respectively. After feature selection, 32 QT features occur at least one time in Lasso, while 10 QT features with a frequency greater than 60 were selected for further analysis, as shown in Table S4 (Appendix C) available in the online supplemental material. Due to the number of SNP features was about 4 times more than QT features, we selected the first 10 top-ranked QT features and the first 40 top-ranked SNP features as input features in our framework (Table 2).

For QT features, left/right hippocampus, left amygdala, right entorhinal cortex, right isthmus cingulate belong to the limbic system. These structures and right middle

TABLE 2
The First 10 Top-Ranked QT and SNP Features

Rank	QT feature	SNP feature
1	Left Hippocampus Volume	rs9289587.Aa
2	Right Entorhinal Thickness	rs1121030.AA
3	Left Inferiorparietal Thickness	rs677737.AA
4	Right Hippocampus Volume	rs205677.AA
5	Left Amygdala Volume	rs429358.AA
6	Right Supramarginal Thickness	rs892601.AA
7	Right Parsorbitalis Thickness	rs17437668.AA
8	Right Middletemporal Thickness	rs3107546.AA
9	Right Isthmuscingulate Thickness	rs6776238.AA
10	Left Fusiform Thickness	rs2051947.AA

 # The full list of the selected SNP features is shown in Table S2 (Appendix B) available in the online supplemental material.

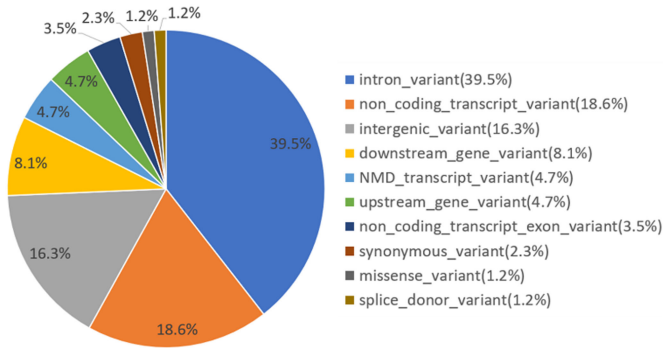

Fig. 3. Percentage of Ensemble Variant Effect Predictor (VEP) consequences of the selected SNP loci. NMD, nonsense-mediated mRNA decay.

temporal belong to the temporal lobe. Left inferior parietal and right supramarginal belong to the parietal lobe. Right pars orbitalis and left fusiform are part of the frontal lobe and occipital lobe, respectively. The selected QT features in our study, especially such as hippocampus volume, amygdala volume, and entorhinal thickness, have been reported as specific biomarkers for MCI classifications in many previous studies [58].

Genetic factors such as SNP also can be used in disease predictions. As far as we know, no study has applied GWAS-based SNP features for MCI classification. The first 40 top-ranked SNP features belong to 39 SNP loci. The selected SNP loci were belonged to 35 corresponding genes, as shown in Table S4 (Appendix C) available in the online supplemental material. Among them, some are putative AD susceptibility genes in previous studies, including *OR5K3* [59], *APOE* [56], *ATXN1* [60], *ADAMTS1* [61] and *SLC10A2* [62]. Some are brain-related or other neurodegeneration disease-related genes, such as *NAPG* [63], *ATP2B2* [64], *ZFPM2* [65], *RUNX1* [66], *CHODL* [67] and *TLE1* [68], being possible candidates for MCI progressive susceptibility. Our selected SNP features may provide an overview of potential genetic mechanisms underlying the heterogeneity of MCI.

To identify the biological significance of the selected SNP loci, we evaluated the effects of all SNP loci on genes, transcripts, and protein sequences, as well as regulatory regions using Ensemble VEP database. Consistent with most studies that most complex disease causal variants are non-coding, only 3.5 percent the selected SNP loci were exonic variants, with the majority were intronic variants (39.5 percent), transcript variants of non-coding RNA genes (18.6 percent) and intergenic variants (16.3 percent) (Fig. 3).

For eQTL analyses, we searched the HaploReg database for cis-acting eQTL of the selected SNP loci (Table S3, Appendix B) available in the online supplemental material. Of these SNP loci, 37 of them have regulatory potential when considering all tissues according to HaploReg database. A total of 19 SNP loci have eQTL information, and four SNP loci are brain-tissue specific eQTLs (Table 3). SNP rs429358 is the most significant risk loci of AD and MCI, and is cis-eQTL for *APOE* expression in the human brain [69]. Rs17437668, rs677911 and rs2261950 are eQTLs for *CCDC53*, *MCOKN2* and HLA-L, respectively. *CCDC53* was related to the dysfunction of retromer. Retromer was reported to play an important role in the pathological mechanism of dementia in

TABLE 3
Brain-Tissue Specific eQTL

Rank	SNP	Tissue	Correlated gene (alias)
5	rs429358	Lymphoblastoid	*APOE*
7	rs17437668	Brain_Hypothalamus	*CCDC53(WASHC3)*
32	rs677911	Brain_Cortex	*MCOLN2(TRPML2)*
36	rs261950	Brain_Hippocampus	*HLA-L*

many researches. Retromer transports amyloid precusor protein (APP) to the surface of neurons to keep them from decomposing into the toxic beta-amyloid protein in the endosomes [70], [71]. *MCOLN2* encodes a mucolipin protein. TRPML1, a homologous gene of *MCOLN2*, has been found through regulating PPARγ/AMPK/Mtor Signalling Pathway involved in the progress of AD [72]. *HLA-L* is a family member of human leukocyte antigen (*HLA*) genes. *HLA* genes have been demonstrated to be involved in the progression and pathogenesis of AD [73].

We searched Braineac database to identify whether these three SNP loci affect corresponding gene expressions or not in ten brain tissues. Significant association between the genotype of rs17437668, rs677911, and *CCDC53*, *MCOLN2* expression level were found (Fig. 4). The T allele

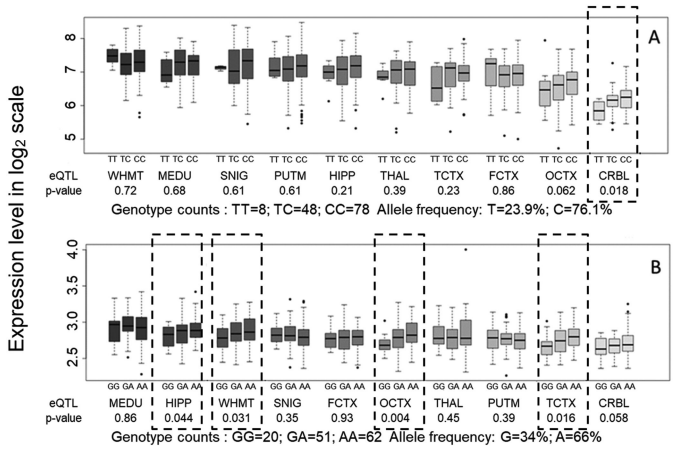

Fig. 4. (A) Effects of rs17437668 genotype on brain *CCDC53* expression level. (B) Effects of rs677911 genotype on brain *MCOLN2* expression level. CRBL, cerebellar cortex; FCTX, frontal cortex; HIPP, hippocampus; MEDU, medulla; OCTX, occipital cortex; PUTM, putamen; SNIG, substantia nigra; TCTX, temporal cortex; THAL, thalamus; WHMT, white matter.

TABLE 4
Significant Reactome Pathway (False Discovery Rate < 0.05)

pathway	description	genes
HSA-983712	Ion channel transport	*ATP2B2,ATP6V1C1,BSND,MCOLN2*
HAS-382551	Transport of small molecules	*ATP2B2,ATP6V1C1,BSND,MCOLN2, APOE,RUNX1,PCSK6*

and especially TT genotype of rs17437668 decreased the *CCDC53* expression in the cerebellar cortex ($p = 0.018$). The G allele and especially GG genotype of rs677911 decreased the *MCOLN2* expressions in the hippocampus ($p = 0.044$), white matter ($p = 0.031$), occipital cortex ($p = 0.004$) and temporal cortex (0.016). Rs261950 is not available in Braineac database.

We also conducted Reactome pathway enrichment analyses of our 35 genes using STRING database [50]. There were two significant Reactome pathways, including ion channel transport (HSA-983712) and transport of small molecules (HSA-382551), as shown in Table 4. "Ion channel transport" is the sub-pathway of "transport of small molecules" in Reactome database. Transport of small molecules across the blood-brain barrier plays an important role in the drug delivery of AD [74]. Besides, Furukawa *et al.* [75] found that the channel proteins on the cell surface are related to AD, and the opening or closing of these channel proteins may be the key to the onset of the AD.

3.3 Classification Performances

First, we built two initial SVM classifiers on 228 original labeled MCI samples from the ADNI-1 cohort using 10 selected QT features and 40 selected SNP features. 20 unlabeled MCI samples were selected from 136 unlabeled MCI samples and utilized in each co-training iteration. After 21 times iterations, 69 unlabeled MCI samples were labeled including 61 pseudo sMCI and 8 pseudo pMCI samples (Appendix D) available in the online supplemental material, and no accordant pseudo samples were observed between QT and SNP classifiers. Finally, random forest algorithm was used to obtain a combined classifier on the 297 labeled MCI samples including 228 original labeled samples and 69 pseudo labeled samples. 83 MCI samples from the ADNI-2 cohort including 62 sMCI and 21 pMCI samples were used as an independent dataset to examine the effectiveness of our methods. The performances of the single modal QT, the single modal SNP, and the combined RF classifiers before and after co-training are listed in Table 5. Accuracy (ACC), sensitivity (SEN), specificity (SPE), precision (PRE) and area under the curve (AUC) were reported in our study. The ROC curves the single modal QT, the single modal SNP and the combined RF classifiers before and after co-training are shown in Fig. 5. The AUC of the combined RF classifier was improved from 0.767 to 0.825 after co-training, as shown in Table 5.

As shown in Table 5, co-training greatly improves the specificity at the price of the sensitivity of combined RF classifier. The sensitivity measures the proportion of correctly identified positive samples (pMCI) while the specificity measures the proportion of correctly identified negative samples (sMCI). For the combined RF classifier before co-training, the potential reason of high sensitivity but low specificity is: many of the sMCI samples are likely to become pMCI and progress to dementia in the near future due to the heterogeneity of MCI [76]. For the combined RF classifier after co-training, the potential reason for the greatly improved specificity at the price of sensitivity is: more pseudo labeled sMCI were selected during co-training processes than pMCI (Table S6, Appendix D) available in the online supplemental material, which made the new labeled dataset class imbalanced. In a class imbalanced dataset, the majority class (sMCI) will have a higher accuracy in prediction and the minority class (pMCI) will have a low accuracy [77]. Considering the low sample size of pMCI, we also reported precision in our study (Table 5). The precision of the combined RF classifier was improved from 47.37 percent to 72.22 percent after co-training.

TABLE 5
Classification Performances of the Classifiers Before and After Co-Training

		ACC (%)	SEN (%)	SPE (%)	PRE (%)	AUC
Before co-training	QT	57.83	90.48	46.77	36.54	0.719
	SNP	75.90	33.33	90.32	53.85	0.607
	RF	72.30	85.70	67.70	47.37	0.767
After co-training	QT	77.11	57.14	83.87	54.55	0.734
	SNP	53.01	76.19	45.16	32.00	0.601
	RF	85.50	76.20	88.70	72.22	0.825

ACC: Accuracy; SEN: Sensitivity; SPE: Specificity; PRE: precision; AUC: Area Under the Curve; QT: quantitative trait; SNP: Single Nucleotide Polymorphism; RF: Random Forest.

We evaluated our model on the 83 independent samples from the ADNI-2 cohort, 70 samples were classified correctly but 13 samples were classified incorrectly. Two possible reasons, the sample labels or the feature data, may lead to the incorrect classifications. One possible reason is that the incorrect classified sMCI samples may progress to dementia, while the incorrect classified pMCI may back to MCI after a short time. Thus, we investigated later-than-36-months' diagnoses of these incorrect classified samples. The results showed that the diagnoses of these samples with later-than-36-months' diagnosis available were consistent with their diagnosis at 36-month's (Table S7; Appendix E)

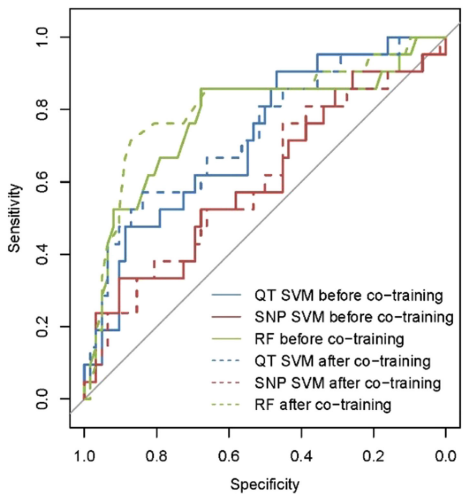

Fig. 5. ROC curves for the QT, SNP, and combined RF classifiers before (solid curve) and after (dashed curve) co-training.

TABLE 6
Comparison of Performances for sMCI/pMCI Classification

Study	N (sMCI,pMCI)	Coversion period (months)	Modality	Validation	ACC (%)	SEN (%)	SPE (%)	AUC
Cho et al. (2012)	203(131,72)	0-18	MRI	Independent dataset	71.0	63.0	76.0	-
Cuingnet et al.(2011)	195(62,133)	0-18	MRI	Independent dataset	67.0	62.0	69.0	-
Zhang et al. (2012)	88(50,38)	0-24	MRI,PET,CSF	Cross validation	78.0	79.0	78.0	0.77
Lebedev et al. (2014)	139(16,123)	0-24	MRI	Independent dataset	82.0	83.0	81.0	-
Beheshti et al.(2017)	136(65,71)	0-36	MRI	Cross validation	75.0	76.9	73.2	0.75
Westman et al.(2012)	162(81,81)	0-36	MRI,PET	Cross validation	68.5	74.1	63.0	0.76
Young et al.(2013)	143(96,47)	0-36	MRI,PET,APOE	Leave one out	74.1	78.7	65.6	0.795
Moradi et al.(2015)	264(100,164)	0-36	MRI	Cross validation	74.7	88.9	51.6	0.766
Hu et al.(2016)	131(62,71)	0-36	MRI	Leave one out	76.7	71.8	82.3	0.79
Hinrichs et al.(2011)	-	0-36	MRI,PET	Leave one out	-	-	-	0.74
Wee et al.(2013)	200(111,89)	0-36	MRI	Independent dataset	75.1	75.1	63.5	0.842
Davatzikos et al.(2011)	239(170,69)	0-36	MRI,CSF	Cross validation	61.7	-	-	0.734
Misra et al. (2009)	103(76,27)	0-36	MRI	Cross validation	82.0	-	-	0.77
Present study	228(115,113)	0-36	MRI,SNP	Independent dataset	85.5	76.2	88.7	0.825

N: Number of samples; Conversion period: length of time over which MCI conversion is defined; MRI: magnetic resonance imaging; ACC: Accuracy; SEN: Sensitivity; SPE: Specificity; AUC: Area under the curve.

available in the online supplemental material. We suspected that the sample labels may not the reason for the incorrect classifications in our study. Another possible reason for the incorrect classifications is that the data distribution of the incorrect classified dataset is more different from the ADNI-1 cohort than the correct classified dataset. A dataset larger than the ADNI-2 cohort should be considered to confirm our hypotheses in future research.

3.4 Comparison With Current Models

In this section, we compared the performances between our method and previously published studies for the prediction of MCI progression (Table 6). We limited the performance comparisons to studies that used omics data from ADNI database. The conversion time which used to define progressive MCI has a strong influence on results [56] and is a part of the heterogeneity of MCI. Therefore, studies with different conversion times were also included in comparisons.

Previously published studies and our present study used different labeling criteria or different modality data or different evaluation methods, which made the performance comparison indirectly when using accuracy metric. Thus, we used AUC, a robust measurement for performance evaluation [78], to compare the performances among our model with other studies. By comparing with similar studies, it can be seen that the performances of our methods are comparable with other studies, even in an independent cohort.

Researchers usually used single-source data, such as MRI, for classifying sMCI and pMCI at different time points of MCI progression. For example, Cho *et al.* [52] and Cuignet *et al.* [79] used 18-months' follow-up as the criterion and MRI data to distinguish sMCI and pMCI (accuracy = 71.0 percent and 67.0 percent). Querbes *et al.* [18] utilized 24-months' follow-up as the criterion and labeled 50 sMCI and 72 pMCI, and used baseline normalized thickness index from MRI to classify sMCI and pMCI (accuracy = 73.0 percent). 36-months' follow-up was a common-used criterion for sMCI/pMCI classifications in many researches. Wee *et al.* [80] used the correlation between the average thickness of the cortical regions of interest to conduct SVM classification and obtained surprisingly high accuracy (AUC = 0.84). Beheshti *et al.* [81] developed a novel diagnosis method that use feature-ranking and a genetic algorithm, and classify MCI using baseline MRI data through standard SVM (AUC = 0.75). Other three studies from Moradi *et al.* [82], Hu *et al.* [83], and Misra *et al.* [84] achieved AUC of 0.766, 0.79, and 0.77 from MRI data, respectively. It has been proved that features from multimodal data share complementary information for disease diagnoses. Zhang *et al.* [85] used 24 months' follow-up and multi-modal data to predict MCI progression and obtained an AUC of 0.77. Westman *et al.* [57] used a multivariate approach that included MRI and PET markers for predicting MCI-to-AD progression and obtained an AUC of 0.76. Young *et al.* [86] also introduced a novel method using Gaussian process classification to classify sMCI and pMCI through integrating MRI, PET and APOE genotype (AUC = 0.73). Hinrichs *et al.* [87] obtained an AUC of 0.74 from MRI and PET data, while Davatzikos *et al.* [76] obtained an AUC of 0.734 from MRI and CSF biomarkers.

4 Conclusions

In summary, we presented a framework with multimodal data using both labeled and unlabeled samples for MCI classification. Our results showed that the combined utilization of sMRI and SNP data through the co-training method could significantly improve the performances of MCI classification in the independent dataset, suggesting that brain structure data and genetic data represent different aspects,

and are complementary to each other. There are two main directions in future work. First, the unlabeled dataset should be much larger than the labeled dataset to allow for better improvements after co-training. However, the number of unlabeled samples was limited in our study and the performance could be improved by using different data sources. The other point was low-quality unlabeled samples might degrade the classification performances, and techniques such as data editing should be used in the identification and elimination of these abnormal samples.

Acknowledgments

Data used in the preparation of this article were obtained from the Alzheimer's Disease Neuroimaging Initiative database (http://www.loni.ucla.edu/ADNI). As such, the investigators within the ADNI contributed to the design and implementation of ADNI and/or provided data but did not participate in analysis or writing of this report. This research was sponsored by the National Natural Science Foundation of China under Grants 81830053, 61972084, and 61872198.

References

[1] R. Lozano *et al.*, "Global and regional mortality from 235 causes of death for 20 age groups in 1990 and 2010: A systematic analysis for the global burden of disease study 2010," *Lancet*, vol. 380, no. 9859, pp. 2095–2128, 2012.

[2] T. F. Hughes, B. E. Snitz, and M. Ganguli, "Should mild cognitive impairment be subtyped?," *Curr. Opi. Psychiatry*, vol. 24, no. 3, pp. 237–242, 2011.

[3] C. Reitz, M.-X. Tang, N. Schupf, J. J. Manly, R. Mayeux, and J. A. Luchsinger, "A summary risk score for the prediction of alzheimer disease in elderly persons," *Archives Neurol.*, vol. 67, no. 7, pp. 835–841, 2010.

[4] S. J. Vos *et al.*, "Prevalence and prognosis of alzheimer's disease at the mild cognitive impairment stage," *Brain*, vol. 138, no. 5, pp. 1327–1338, 2015.

[5] C. Huang *et al.*, "Voxel- and VOI-based analysis of SPECT CBF in relation to clinical and psychological heterogeneity of mild cognitive impairment," *Neuroimage*, vol. 19, no. 3, pp. 1137–1144, 2003.

[6] H. Brodaty, K. Seeher, and L. Gibson, "Dementia time to death: A systematic literature review on survival time and years of life lost in people with dementia," *Int. Psychogeriatrics*, vol. 24, no. 7, pp. 1034–1045, 2012.

[7] Z. Sun, Y. Qiao, B. P. F. Lelieveldt, and M. Staring, "Integrating spatial-anatomical regularization and structure sparsity into SVM: Improving interpretation of Alzheimer's disease classification," *NeuroImage*, vol. 178, pp. 445–460, Sep. 2018.

[8] X. Zhu, H.-I. Suk, L. Wang, S.-W. Lee, and D. Shen, "A novel relational regularization feature selection method for joint regression and classification in AD diagnosis," *Med. Image Anal.*, vol. 38, pp. 205–214, May 2017.

[9] C. Davatzikos, P. Bhatt, L. M. Shaw, K. N. Batmanghelich, and J. Q. Trojanowski, "Prediction of MCI to AD conversion, via MRI, CSF biomarkers, and pattern classification," *Neurobiol. Aging*, vol. 32, no. 12, pp. 2322.e19–2322.e27, Dec. 2011.

[10] C. Salvatore and I. Castiglioni, "A wrapped multi-label classifier for the automatic diagnosis and prognosis of Alzheimer's disease," *J. Neurosci. Methods*, vol. 302, pp. 58–65, 2018.

[11] X. Zhu, H.-I. Suk, S.-W. Lee, and D. Shen, "Discriminative self-representation sparse regression for neuroimaging-based Alzheimer's disease diagnosis," *Brain Imag. Behav.*, vol. 13, no. 1, pp. 27–40, 2019.

[12] G. B. Frisoni, N. C. Fox, C. R. Jack Jr, P. Scheltens, and P. M. Thompson, "The clinical use of structural MRI in alzheimer disease," *Nat. Rev. Neurol.*, vol. 6, no. 2, pp. 67–77, 2010.

[13] C. R. Jack Jr *et al.*, "Hypothetical model of dynamic biomarkers of the alzheimer's pathological cascade," *Lancet Neurol.*, vol. 9, no. 1, pp. 119–128, 2010.

[14] J. C. Stout, M. W. Bondi, T. L. Jernigan, S. L. Archibald, D. C. Delis, and D. P. Salmon, "Regional cerebral volume loss associated with verbal learning and memory in dementia of the Alzheimer type," *Neuropsychology*, vol. 13, no. 2, pp. 188–197, 1999.

[15] A. Fleisher *et al.*, "Volumetric MRI vs clinical predictors of Alzheimer disease in mild cognitive impairment," *Neurology*, vol. 70, no. 3, pp. 191–199, 2008.

[16] G. Karas *et al.*, "Amnestic mild cognitive impairment: Structural MR imaging findings predictive of conversion to Alzheimer disease," *Amer. J. Neuroradiol.*, vol. 29, no. 5, pp. 944–949, 2008.

[17] M. Chupin *et al.*, "Fully automatic hippocampus segmentation and classification in Alzheimer's disease and mild cognitive impairment applied on data from ADNI," *Hippocampus*, vol. 19, no. 6, pp. 579–587, 2009.

[18] O. Querbes *et al.*, "Early diagnosis of Alzheimer's disease using cortical thickness: Impact of cognitive reserve," *Brain*, vol. 132, no. 8, pp. 2036–2047, 2009.

[19] T. S. Wingo, J. J. Lah, A. I. Levey, and D. J. Cutler, "Autosomal recessive causes likely in early-onset Alzheimer disease," *Archive Neurol.*, vol. 69, no. 1, pp. 59–64, 2012.

[20] B. Winblad *et al.*, "Mild cognitive impairment–beyond controversies, towards a consensus: Report of the international working group on mild cognitive impairment," *J. Internal Med.*, vol. 256, no. 3, pp. 240–246, 2004.

[21] R. Hashimoto *et al.*, "Effect of the brain-derived neurotrophic factor and the apolipoprotein e polymorphisms on disease progression in preclinical Alzheimer's disease," *Genes Brain Behav.*, vol. 8, no. 1, pp. 43–52, 2009.

[22] N. T. Lautenschlager, L. Flicker, S. Vasikaran, P. Leedman, and O. P. Almeida, "Subjective memory complaints with and without objective memory impairment: Relationship with risk factors for dementia," *Amer. J. Geriatric Psychiatry*, vol. 13, no. 8, pp. 731–734, 2005.

[23] A. Barabash *et al.*, "APOE, ACT and CHRNA7 genes in the conversion from amnestic mild cognitive impairment to Alzheimer's disease," *Neurobiol. Aging*, vol. 30, no. 8, pp. 1254–1264, Aug. 2009.

[24] K. Ning *et al.*, "Classifying Alzheimer's disease with brain imaging and genetic data using a neural network framework," *Neurobiol. Aging*, vol. 68, pp. 151–158, 2018.

[25] E. Rodríguez-Rodríguez *et al.*, "Genetic risk score predicting accelerated progression from mild cognitive impairment to Alzheimer's disease," *J. Neural Transmiss.*, vol. 120, no. 5, pp. 807–812, 2013.

[26] B. Wang *et al.*, "Similarity network fusion for aggregating data types on a genomic scale," *Nat. Methods*, vol. 11, no. 3, pp. 333–337, 2014.

[27] M. Liu, D. Cheng, K. Wang, Y. Wang, and Alzheimer's Disease Neuroimaging Initiative, "Multi-modality cascaded convolutional neural networks for Alzheimer's disease diagnosis," *Neuroinformatics*, vol. 16, no. 3–4, pp. 295–308, 2018.

[28] F. Schwenker and E. Trentin, "Pattern classification and clustering: A review of partially supervised learning approaches," *Pattern Recognit. Lett.*, vol. 37, pp. 4–14, 2014.

[29] D. Zhang and D. Shen, "Semi-supervised multimodal classification of Alzheimer's disease," in *Proc. IEEE Int. Symp. Biomed. Imag.: Nano Macro*, 2011, pp. 1628–1631.

[30] J. Wu, Y.-B. Diao, M.-L. Li, Y.-P. Fang, and D.-C. Ma, "A semi-supervised learning based method: Laplacian support vector machine used in diabetes disease diagnosis," *Interdisciplinary Sci.: Comput. Life Sci.*, vol. 1, no. 2, pp. 151–155, 2009.

[31] L. An, E. Adeli, M. Liu, J. Zhang, S.-W. Lee, and D. Shen, "A hierarchical feature and sample selection framework and its application for Alzheimer's disease diagnosis," *Sci. Rep.*, vol. 7, pp. 45269, 2017.

[32] A. Blum and T. Mitchell, "Combining labeled and unlabeled data with co-training," in *Proc. 11th Annu. Conf. Comput. Learn. theory*, 1998, pp. 92–100.

[33] W. Sun, T.-L. B. Tseng, J. Zhang, and W. Qian, "Computerized breast cancer analysis system using three stage semi-supervised learning method," *Comput. Methods Programs Biomed.*, vol. 135, pp. 77–88, 2016.

[34] A. B. Zonderman and G. A. Dore, "Risk of dementia after fluctuating mild cognitive impairment: When the yo-yoing stops," *Neurology*, vol. 82, pp. 290–291, 2014.

[35] S. Y. Pandya, M. A. Clem, L. M. Silva, and F. L. Woon, "Does mild cognitive impairment always lead to dementia? A review," *J. Neurol. Sci.*, vol. 369, pp. 57–62, 2016.

[36] M. F. Folstein, S. E. Folstein, and P. R. McHugh, "'Mini-mental state'. A practical method for grading the cognitive state of patients for the clinician.," *J. Psychiatric Res.*, vol. 12 no. 3, pp. 189–198, 1975.
[37] J. C. Morris, "The clinical dementia rating (CDR): Current version and scoring rules.," *Neurology*, vol. 43 no. 11, pp. 2412–2414, 1993.
[38] B. Fischl, "FreeSurfer," *Neuroimage*, vol. 62, no. 2, pp. 774–781, 2012.
[39] J. Barnes *et al.*, "Head size, age and gender adjustment in MRI studies: A necessary nuisance?," *Neuroimage*, vol. 53, no. 4, pp. 1244–1255, 2010.
[40] O. Voevodskaya *et al.*, "The effects of intracranial volume adjustment approaches on multiple regional MRI volumes in healthy aging and Alzheimer's disease," *Front. Aging Neurosci.*, vol. 6, 2014, Art. no. 264.
[41] S. Purcell *et al.*, "PLINK: A tool set for whole-genome association and population-based linkage analyses," *Amer. J. Hum. Genet.*, vol. 81, no. 3, pp. 559–575, 2007.
[42] J. E. Wigginton, D. J. Cutler, and G. R. Abecasis, "A note on exact tests of Hardy-Weinberg equilibrium," *Amer. J. Hum. Genetics*, vol. 76, no. 5, pp. 887–893, 2005.
[43] P. Cerda, G. Varoquaux, and B. Kégl, "Similarity encoding for learning with dirty categorical variables," *Mach. Learn.*, vol. 107, no. 8–10, pp. 1477–1494, 2018.
[44] R. Tibshirani, "Regression shrinkage and selection via the lasso," *J. Roy. Stat. Soc.: Ser. B (Methodol.)*, vol. 58, no. 1, pp. 267–288, 1996.
[45] R. Andonie and A. Cataron, "An informational energy LVQ approach for feature ranking," in *Proc. Eur. Symp. Artif. Neural Netw.*, 2004, pp. 471–476.
[46] L. Breiman, "Random forests," *Mach. Learn.*, vol. 45, no. 1, pp. 5–32, 2001.
[47] W. McLaren *et al.*, "The ensembl variant effect predictor," *Genome Biol.*, vol. 17, no. 1, pp. 122, 2016.
[48] L. D. Ward and M. Kellis, "HaploReg: A resource for exploring chromatin states, conservation, and regulatory motif alterations within sets of genetically linked variants," *Nucleic Acids Res.*, vol. 40, no. D1, pp. D930–D934, 2012.
[49] A. Ramasamy *et al.*, "Genetic variability in the regulation of gene expression in ten regions of the human brain," *Nat. Neurosci.*, vol. 17, no. 10, pp. 1418–1428, 2014.
[50] D. Szklarczyk *et al.*, "STRING v11: Protein–protein association networks with increased coverage, supporting functional discovery in genome-wide experimental datasets," *Nucleic Acids Res.*, vol. 47, no. D1, pp. D607–D613, 2019.
[51] E. Westman *et al.*, "AddNeuroMed and ADNI: Similar patterns of alzheimer's atrophy and automated MRI classification accuracy in Europe and North America," *Neuroimage*, vol. 58, no. 3, pp. 818–828, 2011.
[52] Y. Cho, J.-K. Seong, Y. Jeong, S. Y. Shin, and Alzheimer's Disease Neuroimaging Initiative, "Individual subject classification for Alzheimer's disease based on incremental learning using a spatial frequency representation of cortical thickness data," *Neuroimage*, vol. 59, no. 3, pp. 2217–2230, 2012.
[53] R. Casanova *et al.*, "Alzheimer's disease risk assessment using large-scale machine learning methods," *PLoS One*, vol. 8, no. 11, 2013, Art, no. e77949.
[54] R. Wolz *et al.*, "Multi-method analysis of MRI images in early diagnostics of Alzheimer's disease," *PLoS One*, vol. 6, no. 10, 2011, Art, no. e25446.
[55] B. Cheng *et al.*, "Semi-supervised multimodal relevance vector regression improves cognitive performance estimation from imaging and biological biomarkers," *Neuroinformatics*, vol. 11, no. 3, pp. 339–353, 2013.
[56] J. Young *et al.*, "Accurate multimodal probabilistic prediction of conversion to Alzheimer's disease in patients with mild cognitive impairment," *NeuroImage: Clin.*, vol. 2, pp. 735–745, 2013.
[57] E. Westman, J.-S. Muehlboeck, and A. Simmons, "Combining MRI and CSF measures for classification of Alzheimer's disease and prediction of mild cognitive impairment conversion," *Neuroimage*, vol. 62, no. 1, pp. 229–238, 2012.
[58] M. W. Weiner *et al.*, "The Alzheimer's disease neuroimaging initiative: A review of papers published since its inception," *Alzheimer's Dementia*, vol. 9, no. 5, pp. e111–e194, 2013.
[59] R. L. Doty, "Olfactory dysfunction in neurodegenerative diseases: Is there a common pathological substrate?," *Lancet Neurol.*, vol. 16, no. 6, pp. 478–488, 2017.
[60] K. Bettens *et al.*, "Follow-up study of susceptibility loci for Alzheimer's disease and onset age identified by genome-wide association," *J. Alzheimer's Dis.*, vol. 19, no. 4, pp. 1169–1175, 2010.
[61] B. W. Kunkle *et al.*, "Genetic meta-analysis of diagnosed Alzheimer's disease identifies new risk loci and implicates aβ, tau, immunity and lipid processing," *Nat. Genet.*, vol. 51, no. 3, pp. 414–430, 2019.
[62] J. Mez *et al.*, "Two novel loci, COBL and SLC10A2, for Alzheimer's disease in African Americans," *Alzheimer's Dementia*, vol. 13, no. 2, pp. 119–129, Feb. 2017.
[63] X. Li *et al.*, "Association study on the NAPG gene and bipolar disorder in the Chinese Han population," *Neurosci. Lett.*, vol. 457, no. 3, pp. 159–162, 2009.
[64] W. Yang *et al.*, "The evidence for association of ATP2B2 polymorphisms with Autism in Chinese Han population," *PLoS One*, vol. 8, no. 4, 2013, Art. no. e61021.
[65] L. Greenbaum *et al.*, "Association of the ZFPM2 gene with antipsychotic-induced parkinsonism in schizophrenia patients," *Psychopharmacology*, vol. 220, no. 3, pp. 519–528, 2012.
[66] T. T. Logan, S. Villapol, and A. J. Symes, "TGF-β superfamily gene expression and induction of the runx1 transcription factor in adult neurogenic regions after brain injury," *PloS One*, vol. 8, no. 3, 2013, Art. no. e59250.
[67] A. Enjin *et al.*, "Identification of novel spinal cholinergic genetic subtypes disclose chodl and pitx2 as markers for fast motor neurons and partition cells," *J. Comparative Neurol.*, vol. 518, no. 12, pp. 2284–2304, 2010.
[68] S. G. Dastidar, S. Narayanan, and S. Stifani, and S. R. D'Mello, "Transducin-like enhancer of split-1 (TLE1) combines with forkhead box protein G1 (FoxG1) to promote neuronal survival," *J. Biol. Chem.*, vol. 287, no. 18, pp. 14749–14759, 2012.
[69] T. Lappalainen *et al.*, "Transcriptome and genome sequencing uncovers functional variation in humans," *Nature*, vol. 501, no. 7468, pp. 506–511, 2013.
[70] S. A. Small and G. A. Petsko, "Retromer in Alzheimer disease, parkinson disease and other neurological disorders," *Nat. Rev. Neurosci.*, vol. 16, no. 3, pp. 126–132, 2015.
[71] V. J. Mecozzi *et al.*, "Pharmacological chaperones stabilize retromer to limit APP processing," *Nat. Chem. Biol.*, vol. 10, no. 6, pp. 443–449, 2014.
[72] L. Zhang *et al.*, "TRPML1 participates in the progression of Alzheimer's disease by regulating the PPARγ/AMPK/Mtor signalling pathway," *Cell. Physiol. Biochem.*, vol. 43, no. 6, pp. 2446–2456, 2017.
[73] Z.-X. Wang *et al.*, "Genetic association of HLA gene variants with MRI brain structure in Alzheimer's disease," *Mol. Neurobiol.*, vol. 54, no. 5, pp. 3195–3204, 2017.
[74] W. M. Pardridge, "Transport of small molecules through the blood-brain barrier: Biology and methodology," *Adv. Drug Del. Rev.*, vol. 15, no. 1–3, pp. 5–36, 1995.
[75] J. L. Syrjanen *et al.*, "Structure and assembly of calcium homeostasis modulator proteins," *Nat. Struct. Mol. Biol.*, vol. 27, pp. 150–159, 2020.
[76] C. Davatzikos, P. Bhatt, L. M. Shaw, K. N. Batmanghelich, and J. Q. Trojanowski, "Prediction of MCI to AD conversion, via MRI, CSF biomarkers, and pattern classification," *Neurobiol. Aging*, vol. 32, no. 12, pp. 2322–e19, 2011.
[77] W.-J. Lin and J. J. Chen, "Class-imbalanced classifiers for high-dimensional data," *Brief. Bioinf.*, vol. 14, no. 1, pp. 13–26, 2013.
[78] S. F. Eskildsen, P. Coupé, D. García-Lorenzo, V. Fonov, J. C. Pruessner, and D. L. Collins, "Prediction of Alzheimer's disease in subjects with mild cognitive impairment from the ADNI cohort using patterns of cortical thinning," *NeuroImage*, vol. 65, pp. 511–521, Jan. 2013.
[79] R. Cuingnet *et al.*, "Automatic classification of patients with Alzheimer's disease from structural MRI: A comparison of ten methods using the ADNI database," *Neuroimage*, vol. 56, no. 2, pp. 766–781, 2011.
[80] C.-Y. Wee, P.-T. Yap, and D. Shen, and Alzheimer's Disease Neuroimaging Initiative, "Prediction of Alzheimer's disease and mild cognitive impairment using cortical morphological patterns," *Hum. Brain Mapping*, vol. 34, no. 12, pp. 3411–3425, 2013.
[81] I. Beheshti, H. Demirel, and H. Matsuda, "Classification of alzheimer's disease and prediction of mild cognitive impairment-to-Alzheimer's conversion from structural magnetic resource imaging using feature ranking and a genetic algorithm," *Comput. Biol. Med.*, vol. 83, pp. 109–119, 2017.

[82] E. Moradi *et al.*, "Machine learning framework for early MRI-based Alzheimer's conversion prediction in MCI subjects," *Neuroimage*, vol. 104, pp. 398–412, 2015.
[83] K. Hu, Y. Wang, K. Chen, L. Hou, and X. Zhang, "Multi-scale features extraction from baseline structure MRI for MCI patient classification and AD early diagnosis," *Neurocomputing*, vol. 175, pp. 132–145, 2016.
[84] C. Misra, Y. Fan, and C. Davatzikos, "Baseline and longitudinal patterns of brain atrophy in MCI patients, and their use in prediction of short-term conversion to AD: Results from ADNI," *Neuroimage*, vol. 44, no. 4, pp. 1415–1422, 2009.
[85] D. Zhang and D. Shen, and Alzheimer's Disease Neuroimaging Initiative, "Multi-modal multi-task learning for joint prediction of multiple regression and classification variables in Alzheimer's disease," *NeuroImage*, vol. 59, no. 2, pp. 895–907, 2012.
[86] J. Young *et al.*, "Accurate multimodal probabilistic prediction of conversion to Alzheimer's disease in patients with mild cognitive impairment," *NeuroImage: Clin.*, vol. 2, pp. 735–745, 2013.
[87] C. Hinrichs, V. Singh, G. Xu, S. C. Johnson, and Alzheimer's Disease Neuroimaging Initiative, "Predictive markers for AD in a multi-modality framework: An analysis of MCI progression in the ADNI population," *Neuroimage*, vol. 55, no. 2, pp. 574–589, 2011.

Shaoxun Yuan received the master's degree in biology from Nanjing Agricultural University, in 2015. He is currently working toward the PhD degree in Southeast University. His main research interests includes imaging genetics and machine learning.

Haitao Li received the master's degree in communication and information system from Qufu Normal University, in 2016. He is currently working toward the PhD degree in Southeast University. His main research interests includes machine learning and bioinformatics.

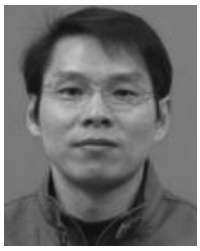

Jiansheng Wu received the BS degree in bioengineering, from Nanchang University, in 2000, the MS degree, in ecology, from East China Normal University, in 2004, and the PhD degree in biomedical engineering, from Southeast University, China, in 2009. He joined the School of Geography and Biological Information of Nanjing University of Posts and Telecommunications, China, in 2009. His research interests include machine learning and bioinformatics. In these areas he has published more than 20 papers in leading journals and conference proceedings.

Xiao Sun received the BS degree in computer science, from Southeast University, in 1984, and the PhD degree in biomedical engineering, from Southeast University, in 1993. Since 2001, he has been a professor in the School of Biological Science and Medical Engineering of Southeast University. His major research interests include bioinformatics and biomedical big data. He has been in charge of and completed many projects which were funded by the Natural Science Foundation of China, National High-tech R&D Program (863 Program) or National key Basic Research Program of China (973 program). He is the author or corresponding author of more than 100 papers. He also published two books "*Fundamentals of Bioinformatics*" and "*R & BioConductor and Their Applications in Genome Analysis*".